Physics Letters A 384 (2020) 126570

Contents lists available at ScienceDirect

Physics Letters A

www.elsevier.com/locate/pla

Bosonic topological insulator intermediate state in the superconductor-insulator transition

M.C. Diamantini [a], A.Yu. Mironov [b,c], S.M. Postolova [b,d], X. Liu [e], Z. Hao [e], D.M. Silevitch [f], Ya. Kopelevich [g], P. Kim [e], C.A. Trugenberger [h], V.M. Vinokur [i,j,*]

[a] NiPS Laboratory, INFN and Dipartimento di Fisica e Geologia, University of Perugia, via A. Pascoli, I-06100 Perugia, Italy
[b] A.V. Rzhanov Institute of Semiconductor Physics SB RAS, 13 Lavrentjev Avenue, Novosibirsk 630090, Russia
[c] Novosibirsk State University, Pirogova str. 2, Novosibirsk 630090, Russia
[d] Institute for Physics of Microstructures RAS, GSP-105, Nizhny Novgorod 603950, Russia
[e] Department of Physics, Harvard University, Cambridge, MA 02138, USA
[f] Division of Physics, Mathematics, and Astronomy, California Institute of Technology, Pasadena, CA 91125, USA
[g] Universidade Estadual de Campinas-UNICAMP, Instituto de Física "Gleb Wataghin"/DFA, Rua Sergio Buarque de Holanda, 777, Brazil
[h] SwissScientific Technologies SA, rue du Rhone 59, CH-1204 Geneva, Switzerland
[i] Materials Science Division, Argonne National Laboratory, 9700 S. Cass Avenue, Lemont, IL 60637, USA
[j] Consortium for Advanced Science and Engineering (CASE), University of Chicago, 5801 S Ellis Ave, Chicago, IL 60637, USA

A R T I C L E I N F O

Article history:
Received 12 April 2020
Accepted 12 May 2020
Available online 19 May 2020
Communicated by L. Ghivelder

Keywords:
Berezinskii-Kosterlitz-Thouless transition
Superconductor-insulator transition
Bose metal
Bosonic topological insulator
Josephson junction arrays
Quantum Berezinskii-Kosterlitz-Thouless transition

A B S T R A C T

A low-temperature intervening metallic regime arising in the two-dimensional superconductor-insulator transition challenges our understanding of electronic fluids. Here we develop a gauge theory revealing that this emergent anomalous metal is a bosonic topological insulator where bulk transport is suppressed by mutual statistics interactions between out-of-condensate Cooper pairs and vortices and the longitudinal conductivity is mediated by symmetry-protected gapless edge modes. We explore the magnetic-field-driven superconductor-insulator transition in a niobium titanium nitride device and find marked signatures of a bosonic topological insulator behavior of the intervening regime with the saturating resistance. The observed superconductor-anomalous metal and insulator-anomalous metal dual phase transitions exhibit quantum Berezinskii-Kosterlitz-Thouless criticality in accord with the gauge theory.

Introduction

An anomalous metallic regime intervening between the superconductor and insulator has been reported in a wide variety of two-dimensional electronic systems experiencing the superconductor-to-insulator transition (SIT) [1–15], and is often referred to as "Bose metal" [16]. Despite decades of dedicated studies [17,18], its nature remains unclear and poses a challenge to our understanding of electron fluids. The very existence of a 2D metal is at odds with the 2D orthodoxy, as conventional theories expect a direct quantum SIT with no intermediate metallic phase.

Yet a gauge theory of Josephson junction arrays (JJA) at $T = 0$ [19] predicted a metallic phase intervening between the superconductor and superinsulator at $T = 0$. Extending the approach of [19] to finite temperatures, enabled us to develop a field theory of the SIT [20] and unravel the fundamental role of the infrared-dominant Aharonov-Bohm-Casher (ABC) mutual statistics interactions that determine the SIT phase structure. Here utilizing the technique of [20], we construct a gauge theory of the Bose metal (BM) in which strong quantum fluctuations prevent Bose condensation of both vortices and Cooper pairs (CP) and their mutual statistics interactions, see Fig. 1, induce a gap in their fluctuation spectrum, quantified by the Chern-Simons mass, m_{cs} [21], preventing bulk transport. The longitudinal conductance is mediated by symmetry-protected $\mathrm{U}(1)\times\mathbb{Z}_2^{\mathrm{T}}$ edge modes, where $\mathbb{Z}_2^{\mathrm{T}}$ denotes time-reversal symmetry. Hence the BM realizes the long sought [22] bosonic topological insulator. We demonstrate that at $T = 0$ the transitions between the superconductor and BM and between the BM and superinsulator are the respective quantum Berezinskii-Kosterlitz-Thouless (BKT) transitions. We report transport measurements on niobium titanium nitride (NbTiN) and van der Waals heterostructures of twisted double bilayer graphene (TDBG) films offering strong support to the proposed picture.

* Corresponding author.
E-mail address: vinokour@anl.gov (V.M. Vinokur).

https://doi.org/10.1016/j.physleta.2020.126570

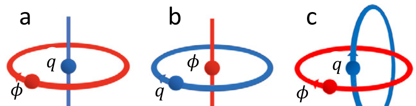

Fig. 1. Mutual statistics interactions. a: A charge (blue ball) evolves along the Euclidean time axis and is encircled by a vortex (red). The two trajectories are topologically linked since one cannot decouple the charge trajectory from the circle without breaking it. This linking encodes the Aharonov-Casher effect. **b:** A dual situation in which a vortex (red ball) evolves along the Euclidean time direction and is encircled by a charge. This linking represent the Aharonov-Bohm effect. **c:** The linked charge-anticharge and vortex-antivortex fluctuations representing coupled Aharonov-Bohm-Casher interactions which are encoded in the Chern-Simons term in the action. (For interpretation of the colors in the figure(s), the reader is referred to the web version of this article.)

Phase structure of the SIT

We consider a two-dimensional superconducting film in the vicinity of the SIT at temperatures $T \leqslant T_{c0}$, where T_{c0} is the mean-field temperature of formation of Cooper pairs with the infinite lifetime. Near the SIT, a film acquires self-induced electronic granularity which, conjectured in [23,24], became a paradigmatic attribute of the SIT [25,26]. This implies that in the critical vicinity of the SIT the 2D superconducting film can be perfectly modeled as the granular superconductor or JJA. The latter harbors interacting elementary excitations, Cooper pairs which in this case can be considered as charged bosons [27,28] and vortices with characteristic energies $4E_{\mathrm{C}}$ and $2\pi^2 E_{\mathrm{J}}$, respectively, E_{C} and E_{J} being the charging energy and Josephson coupling energy of a single junction. The mapping on the real film is achieved by replacement $4E_{\mathrm{C}} \to e_{\mathrm{q}}^2 = 4e^2/\ell$ and $2\pi^2 E_{\mathrm{J}} \to e_{\mathrm{v}}^2 = \Phi_0^2/\lambda_\perp$ where e is the electron charge (we use natural units, $c = 1$, $\hbar = 1$, restoring physical units when necessary), $\Phi_0 = \pi/e$ is the flux quantum, the ultraviolet (UV) cutoff of the theory is defined as $\ell \simeq \min\{d, \xi\}$, with d and ξ being the thickness of the film and the superconducting coherence length, respectively, and $\lambda_\perp = \lambda_{\mathrm{L}}^2/d$ is the Pearl length of the film, with λ_{L} being the London penetration depth of the bulk material. Note that in a superconducting film the mean distance between Cooper pairs is much less than the size of a single Cooper pair, hence, strictly speaking, the latter are not bosons. However, since in a superconducting film the Cooper pair condensate maintains phase coherence, one can still describe the ensemble of Cooper pairs interacting with vortices and an ensemble of bosons [28,29]. Furthermore, since $E_{\mathrm{J}} \sim g\Delta$, where Δ is the gap in a superconducting granule in the JJA and g is the dimensionless tunneling conductance between the adjacent granules, the model implicitly takes into account dissipation effects.

The behavior of an ensemble of interacting vortices and CP near the SIT is governed by the free energy which we derive from the mixed Chern-Simons action [20], explicitly accounting for the ABC effects [21,30]. To that end we integrate out the gauge fields and arrive at the free energy of a system of strings carrying electric and magnetic quantum numbers Q and M and representing the Euclidean trajectories of charges and vortices on a lattice of spacing ℓ, see Methods and Supplementary Information (SI): $\mathcal{F} = \left(Q^2/g + gM^2 - 1/\eta\right)\mu_{\mathrm{e}}\eta N$, where the string length $L = N\ell$ and $g = e_{\mathrm{v}}/e_{\mathrm{q}} = (\pi/e^2)\sqrt{\ell/\lambda_\perp}$ is the dimensionless tuning parameter with $g = g_{\mathrm{c}} = 1$ corresponding to the SIT. In experiments on films experiencing the disorder-driven SIT, the tuning parameter is the dimensionless conductance, $g = R_{\mathrm{Q}}/R_0$, where $R_{\mathrm{Q}} = h/4e^2$ is the quantum resistance for CP, h is the Planck constant, and R_0 is the sheet resistance of the film measured at predefined standard conditions. The parameter g describes thus the tuning of the SIT not only by regulating disorder, but implicitly also by varying dissipation [31] (in JJA $g = \sqrt{(\pi^2/2)(E_{\mathrm{J}}/E_{\mathrm{C}})}$). The dimensionless parameter η describes the strength of quantum fluctuations. Near the SIT, where $e_{\mathrm{q}} \approx e_{\mathrm{v}}$, η acquires the form (in physical units)

$$\eta = \frac{1}{\alpha}\frac{\pi^2\ell}{\mu_{\mathrm{e}}\lambda_\perp}\, G\left(\frac{\pi\ell}{\alpha\lambda_\perp}\right), \tag{1}$$

where $\alpha = e^2/(\hbar c) \approx 1/137$ is the fine structure constant, μ_e is the positional entropy (see SI), and G is the diagonal element of the 3D Green function describing electromagnetic interactions screened by the CS mass, see SI. Identifying the UV cutoff with the superconducting coherence length ξ, yields the geometric factor as $d/(\kappa\lambda_{\mathrm{L}})$ where $\kappa = \lambda_{\mathrm{L}}/\xi$ is the Landau-Ginzburg parameter.

Bose condensation of charges and/or vortices means proliferation of strings of an arbitrary size and occurs if $\mathcal{F}$ is negative, i.e. if

$$Q^2/g + gM^2 < 1/\eta\,. \tag{2}$$

The phase emerging at particular values of g and η is determined by the geometric condition that the nods on a square lattice of integer electric and magnetic charges, $\{Q, M\}$, fall within the interior of an ellipse with semi-axes $r_{\mathrm{Q}} = (g/\eta)^{1/2}$ and $r_{\mathrm{M}} = 1/(g\eta)^{1/2}$, see Fig. 2(a–d). The Bose metal emerges if none of the condensates can form i.e. if simultaneously

$$g/\eta > 1 \text{ and } g\eta > 1\,. \tag{3}$$

This relation resolves the enigma of why some materials exhibit a direct SIT while others go through the intermediate Bose metal phase. The direct SIT at $g = 1$ corresponds to $\eta < 1$; tuning g, one crosses the region $\eta < g < 1/\eta$, where both vortex and Cooper pair condensates coexist, i.e. the direct SIT is a first-order quantum transition. The Bose metal phase opens up for $\eta > 1$ and is favored by thicker films and for materials with low κ. Its domain is delimited by the lines $g = \eta$ and $g = 1/\eta$. As we show below, these lines represent quantum BKT transitions [32,33], and $g = 1$, $\eta = 1$ is a quantum tri-critical point.

To describe the magnetic-field-driven SIT in systems with $g \approx 1$ i.e. which are already on the brink of the SIT, we introduce the frustration factor $f = B/B_\Phi$, where B_Φ is the magnetic field corresponding to one flux quantum $\Phi_0 = \pi/e$ per unit cell. Then the external magnetic field shifts $M \to M + f$ and modifies the condensation conditions, see Fig. 2e,f. Setting $g = 1 + \epsilon$, with $\epsilon \ll 1$, one finds for a direct SIT at $\eta < 1$, $f_{\mathrm{c}} = (1/2)(g^2 - 1) \approx \epsilon$. At $\eta > 1$, but still close to the tri-critical point, one sets $g = \eta + \epsilon$ and obtains for the superconductor-BM transition $f_{\mathrm{c}} = \sqrt{\epsilon}/\eta^{3/2} = (g - \eta)^{1/2}/\eta^{3/2}$ see SI for details.

The nature of the intermediate Bose metal

The response of a BM to an applied field is determined by its effective electromagnetic action, obtained by integrating out the effective gauge fields in the general Chern-Simons action (see Methods), which (without any loss of generality) assumes the simplest form in the relativistic case

$$S_{\mathrm{eff}}\left(A_\mu\right) = \frac{g}{2}\left(\frac{\bar{q}e}{2\pi}\right)^2 d \int d^3x\, A_\mu \left(-\delta_{\mu\nu}\nabla^2 + \partial_\mu\partial_\nu\right) A_\nu\,, \tag{4}$$

where A_μ is the external electromagnetic potential, the dimensionless charge unit $\bar{q} = 2$ for CP and the renormalized effective charge $\bar{q}e_{\mathrm{eff}} = \bar{q}e\sqrt{g}$. Accordingly, the charge current j_μ is found as $j^\mu_{\mathrm{ind}} = (\delta/\delta A_\mu) S_{\mathrm{eff}}(A_\nu) = g\,(\bar{q}e/2\pi)^2 d\ \partial_\nu F^{\mu\nu}$, with $F_{\mu\nu} = \partial_\mu A_\nu - \partial_\nu A_\mu$. One sees that only the derivatives of the external fields, but not their constant parts, induce a current. Therefore, in the bulk, both the longitudinal and the quantum Hall components of the linear conductance vanish at $T = 0$.

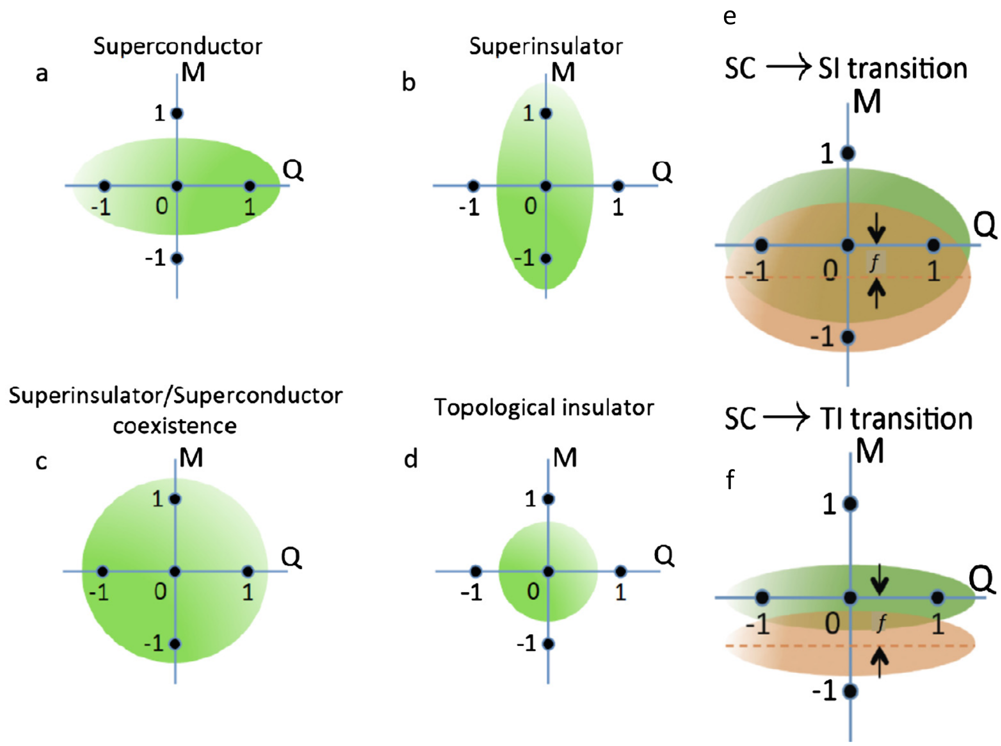

Fig. 2. Graphic representation of the conditions for realizing different phases near the SIT. a: Superconductor: Strings with electric quantum numbers condense. **b:** Superinsulator: Strings with magnetic quantum numbers condense. **c:** Coexistence of long electric and magnetic strings near the first-order direct transition from a superconductor to a superinsulator. **d:** Bosonic topological insulator/Bose metal: all strings are suppressed by their high self-energy. **e:** Phase transitions induced by an external magnetic field: Direct, magnetic-field-induced transition from a superconductor to a superinsulator for $\eta < 1$. **f:** Magnetic-field-driven transition from a superconductor to a topological insulator for $\eta > 1$.

However, the Chern-Simons effective action is not invariant under gauge transformations not vanishing on the sample boundaries. To restore the gauge invariance, one has to add edge chiral bosons [34]. This operation is an exact analogue to the description of the edge modes in the quantum Hall effect [35]. The resulting edge action gives rise to the equation of motion, see Methods and SI:

$$v_{\mathrm{b}}\rho = \frac{\bar{q}e_{\mathrm{eff}}}{2\pi}V \, , \tag{5}$$

where v_{b} is the velocity of the edge modes and V is the applied voltage. Using $I = \bar{q}e_{\mathrm{eff}}v_{\mathrm{b}}\rho$, one finds the longitudinal sheet resistance

$$R_{\square} \equiv \frac{V}{I} = \frac{R_{\mathrm{Q}}}{g} \, , \tag{6}$$

which is in a full concert with the early elegant charge-vortex duality arguments [31,36] leading to $R_{\square} = R_{\mathrm{Q}}$ [36,37] at the SIT. In experiments, $R_{\square}$ may well deviate from R_{Q} upon departure from the SIT, but the standard SIT scaling analysis yields the convergence of $R_{\square}(T \to 0)$ to R_{Q} [2,3,15] upon approach to the presumed quantum critical point. At zero temperature and $\eta > 1$, the Bose metal forms between the points $g = 1/\eta$ and $g = \eta$. Hence its sheet resistance is lower than the quantum resistance, $R_{\square} < R_{\mathrm{Q}}$, on the superconducting side, $g > 1$, and larger than the quantum resistance, $R_{\square} > R_{\mathrm{Q}}$, on the insulating side, $g < 1$, with equality achieved at $g = 1$. Duality is realized in the form $R_{\mathrm{Q}}/R_{\square} \leftrightarrow R_{\square}/R_{\mathrm{Q}}$ when $g \leftrightarrow 1/g$, generalizing the universality arguments of [31,36,37] onto the Bose metal.

Bulk transport suppressed by the topological gap and ballistic symmetry-protected edge modes are the hallmark of topological insulators. In our case, while the flux quantum is π/e, the charge is carried by bosonic excitations of charge $2e$. The BM is thus an integer bosonic topological insulator with edge modes protected by the $\mathrm{U}(1) \rtimes \mathbb{Z}_2^{\mathrm{T}}$ symmetry. This is one of the generic integer topological phases recently classified in [38,39]. The quantum fluctuations parameter η, the suppression of bulk conductances by the topological CS mass m_{CS}, and equations (5, 6) for the longitudinal resistivity mediated by the $\mathrm{U}(1) \rtimes \mathbb{Z}_2^{\mathrm{T}}$-symmetry protected gapless edge states are the central results of our work.

Shown in Fig. 3a is a 3D sketch of the phase diagram comprising the BM near the SIT, with the tuning parameter g denoting either the conductance, or magnetic field or gate voltage in a proximity array [15]. The BM forms at $\eta > 1$ and occupies the domain between the charge- and vortex-BKT transition manifolds. Fig. 3b is a $= 0$ cut of the phase diagram. At $\eta < 1$, the direct SIT is a first-order transition. The lines $\eta = 1/g$ at $\eta > 1, g < 1$ and $\eta = g$ at $\eta > 1, g > 1$, denote quantum BKT transitions between superinsulator and BM and between BM and superconductor, respectively, see SI for detail. Shown in Fig. 3c is g, T-phase diagram corresponding to some $\eta = 1$. Quantum transitions between the superinsulator and the BM and between the superconductor and the BM at $T = 0$ occur at $g = g_1(\eta)$, and $g = g_2(\eta)$, respectively. Duality requires $g_2 = 1/g_1$. By self-duality, the remnant of the SIT can still be identified as $g = 1$ line at which $R_{\square}(T) = R_Q$. And although there is no phase transition anymore at this point, the BKT criticality is still expected in the vicinity of the tricritical point $g = 1$, $\eta = 1$, see below.

Stability of the bosonic topological insulator

To unravel the mechanism preventing the condensation of CP and ensuring stability of the Bose metal, we recall that the particle number operator N_q and the U(1) phase φ, form a pair of canonically conjugate variables, since N_{q} is the generator of global U(1) charge transformations. Only two symmetry realizations are allowed in infinite systems. Either (i) N_{q} is sharp, $\Delta N_{\mathrm{q}} =$

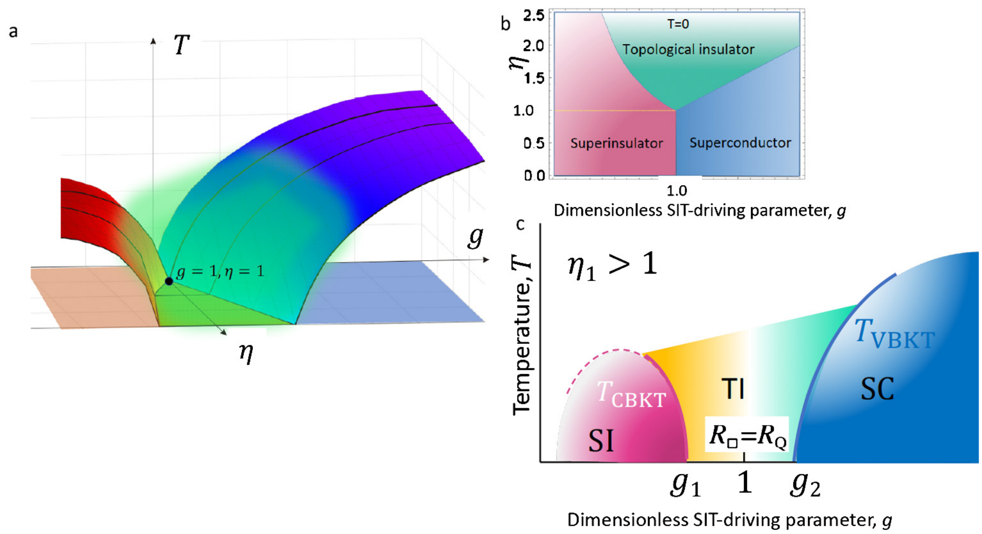

Fig. 3. Phase structure of the SIT. a: Three-dimensional sketch of the phase diagram near the SIT in (g, η, T) coordinates. The red and blue surfaces represent the loci for charge and vortex BKT transitions, the green "cloud" depicts the domain of the Bose metal, which is shown (see text) to be a bosonic topological insulator, hence marked as TI. **b:** Zero temperature cut of the phase diagram. **c:** A cut at $\eta > 1$, representing the schematic phase diagram for strong quantum fluctuations (not to scale) near the SIT. The topological insulator (TI) state is separated from the superconducting (SC) and superinsulating (SI) states by vortex- and charge-BKT transitions respectively (magenta and blue solid lines respectively). In the vicinity of the T_{VBKT} line, $R_\square < R_\mathrm{Q}$ and the system exhibits metallic behavior which crosses over smoothly into the thermally activated insulating behavior upon decreasing g shown by the change of the color. At $g=1$, $R_\square = R_\mathrm{Q}$ and the resistance keeps increasing, $R_\square > R_\mathrm{Q}$, towards the T_{CBKT} line. The yellow strip depicts the domain of thermally activated resistance, which crosses over to BKT critical behavior on approach to T_{CBKT}. The SIT-driving values g_1 and g_2 that mark superinsulator-Bose metal and superinsulator-Bose metal quantum transitions satisfy the duality relation $g_2 = 1/g_1$. The parameter g can be either the dimensionless conductance of the film, or magnetic field, or gate voltage in the gate-driven SIT.

$\sqrt{\langle (N_\mathrm{q} - \bar{N}_\mathrm{q})^2 \rangle} = 0$, and φ is undefined, $\Delta\varphi = \infty$ so that the U(1) symmetry is linearly realized, or (ii) N_q does not annihilate the vacuum, $\Delta N_\mathrm{q} = \infty$, φ is sharp, $\Delta\varphi = 0$ and the global U(1) symmetry is spontaneously broken. When φ is a massless field, these two possibilities define the zero-temperature superinsulators and superconductors [24,40]. However, because of the topological Chern-Simons interactions, the charge and vortex densities do not obey anymore the Gauss-law constraints generating the two U(1) symmetries, and the third possibility, $\Delta N_\mathrm{q} = 0$, φ massive, arises. We find that in the Bose metal, the equal-time quantum correlation functions in the ground state are given by (see SI)

$$\begin{aligned} \langle j^0(\mathbf{x}) j^0(\mathbf{y}) \rangle &\propto \exp\left(-\frac{|\mathbf{x}-\mathbf{y}|}{\xi_{\mathrm{corr}}(g/g_1)}\right) \\ \langle \phi^0(\mathbf{x}) \phi^0(\mathbf{y}) \rangle &\propto \exp\left(-\frac{|\mathbf{x}-\mathbf{y}|}{\xi_{\mathrm{corr}}(g_2/g)}\right), \end{aligned} \tag{7}$$

where j^0 and ϕ^0 are the charge and vortex densities, respectively and

$$\xi_{\mathrm{corr}}(x) \propto \exp(\mathrm{const}/\sqrt{|x-1|}),$$

is the BKT [32,33] correlation length with x set by the quantum coupling constant g and its critical point g_c. Accordingly, the two dual transitions, superconductor-BM and superinsulator-BM are quantum BKT transitions. Another far-reaching implication of Eq. (7) is that charges and vortices form an intertwined liquid comprising fluctuating macroscopic islands with typical dimensions $\xi(g/g_1)$ and $\xi(g_2/g)$, respectively. The emergent texture is referred to as the self-induced electronic granularity [40]. The associated characteristic frequency of the BM quantum fluctuations is $\omega = v/\xi_{\mathrm{corr}}$. While the exact expression for the correlation length in the ground state is not yet available, it must lie in the interval $\xi < \xi_{\mathrm{corr}} < \hbar/(v m_{\mathrm{CS}})$, where the upper bound is the length scale associated with the CS gap to the first excited state. We obtain thus for the frequency range $\omega > m_{\mathrm{CS}} v^2/\hbar$. Using $m_{\mathrm{CS}} = \hbar e_\mathrm{q} e_\mathrm{v}/\pi v$ and $e_\mathrm{v} \approx e_\mathrm{q}$ at the center of the BM phase, we find $\omega > \alpha v/d$. This is the typical frequency associated with the electrostatic energy $\hbar\alpha v/d$ of a Cooper pair. For the NbTiN parameters [41] $d = 10$ nm and $v/c = 1/\sqrt{\varepsilon} = 1/\sqrt{800}$, we find $\omega > 7$ THz.

Experiment

Transport measurements are taken on NbTiN 10 nm thick films prepared by the atomic layer deposition (ALD) technique based on sequential surface reaction, step-by-step film growth. The films were lithographically patterned into bars, see Fig. 4a, and resistivity measurements were performed at sub-Kelvin temperatures in helium dilution refrigerators (see the details of the sample preparation, geometry, measurement technique and characterization in [41]). All the resistance measurements were carried out in the linear regime. In our measurements we used a system of filters built into the cryostat that cuts off the signal above 100 kHz and a system of external filters that cut off the signal above 30 Hz. In addition, wires with high-quality shielding were used for measurements, as well as individual grounding of the measuring circuit. The magnetic field dependence of the saturation resistance, see Fig. 4b, rules out the possibility that the metallic state results from inadequate filtering. Since the expected frequency of typical quantum fluctuations responsible for BM behaviour exceeds by several orders of magnitude the system of filtration, this is effective for noise elimination but does not affect the relevant physics at higher frequencies. Shown in Fig. 4a is the sketch of the two-terminal setup. Fig. 4b presents the log-log plot of the low-temperature part of $R_\square(T)$ across the magnetic field-driven SIT. At magnetic fields $B \lesssim 0.04$ T, $R_\square$ saturates at lowest measured temperatures to the magnetic field-dependent value spanning about an order of magnitude in sheet resistance, from $R_\square \simeq 1$ kΩ to $R_\square \simeq 20$ kΩ, suggesting metallic behaviour across this range. At fields above $B \simeq 0.011$ T, the $R_\square(T)$ dependence develops a minimum. Above $B \gtrsim 0.04$ T, the curve shows a trend to an insulating upturn, and, as soon as B exceeds 0.16 T, $R_\square(T)$ exhibits pronounced insulating behaviour. Plotting $R_\square(B)$ isotherms, see panel Fig. 4c, exposes three sequential crossing points $B_{\mathrm{SB}} = 0.011 \pm 0.001$ T, $B_{\mathrm{SI}} = 0.039 \pm 0.001$ T, and $B_{\mathrm{IB}} = 0.16 \pm 0.01$ T. The correspond-

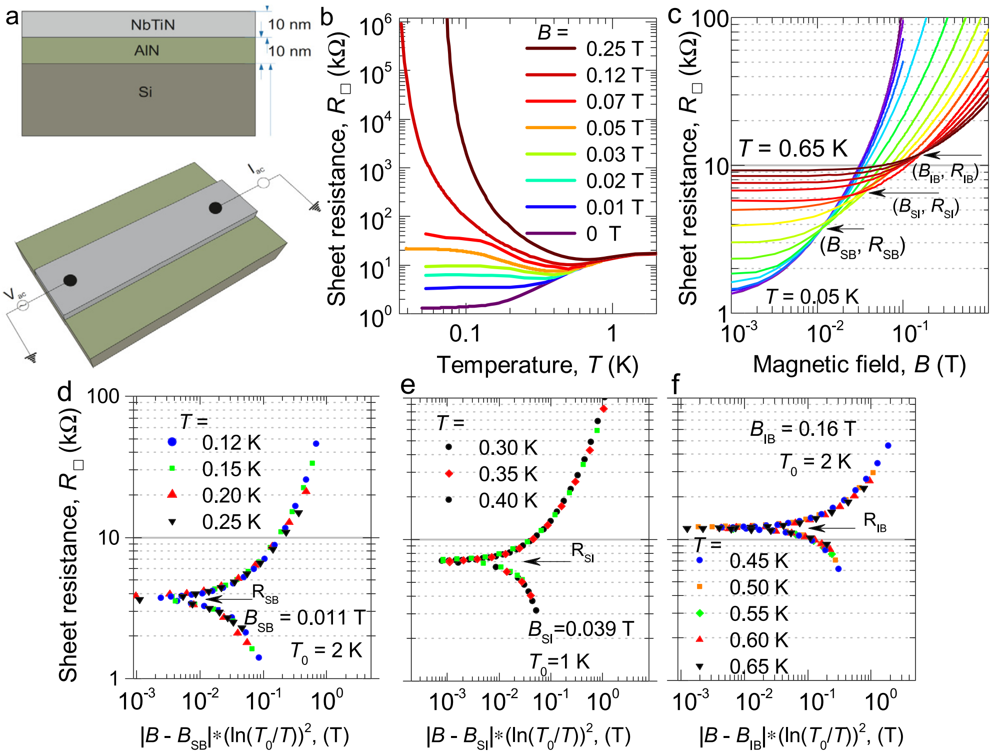

Fig. 4. Temperature and magnetic field dependencies and quantum BKT scaling of $R_\square(T, B)$ in the vicinity of the magnetic field-driven SIT. a: The device scheme and a setup for the two-terminal resistance measurements sketch. **b:** Sheet resistance, $R_\square$, as function of temperature, T, spanning the anomalous metallic regime in the magnetic field range from 0 T to 0.25 T. The residual resistance grows with decreasing g and becomes $R_\square = R_Q$ at $g \simeq 1$. **c:** Sheet resistance, $R_\square$, as function of B for different temperatures exhibits three crossing points (marked by arrows) at $B_{SB} = 0.011$ T, $B_{IB} = 0.16$ T, and $B_{SI} = 0.039$ T, corresponding to superconductor-BM, BM-superinsulator, and the SIT transitions, respectively. The crossing points satisfy the duality relation $B_{SB}/B_{SI} = B_{SI}/B_{IB}$ with great accuracy. **d:** Quantum BKT scaling near the B_{SB} critical point. **e:** The BKT scaling for the remnant of the SIT. **f:** Quantum BKT scaling near the B_{IB} critical point.

ing resistances are $R_{SB} = 3.63 \pm 0.01$ kΩ, $R_{SI} = 6.57 \pm 0.01$ kΩ, and $R_{SI} = 11.9 \pm 0.1$ kΩ.

Temperature dependencies of the resistance $R(T)$ of TDBG measured at optimal doping in the presence of the magnetic field, $B_{||}$, parallel to the film indicates the field-induced SIT, see [42], where also the details of fabrication of TDBG devices and measurements protocol can be found. In the intermediate $B_{||}$ region $R(T)$ develops a minimum the position of which depends on $B_{||}$. As we discuss below, these minima may indicate the possibility of the formation of the bosonic topological insulator state.

Discussion and conclusion

The developed gauge theory establishes a consistent picture of the SIT and the intervening Bose metal state. Materials harboring weak quantum fluctuations experience a direct transition. Materials hosting enhanced quantum fluctuations, sufficient to destroy both Cooper pair and vortex Bose condensates, exhibit the SIT via an intermediate Bose metallic state. The strength of quantum fluctuations is quantified by the parameter η defined in Eq. (1). The Bose metal state is a bosonic topological insulator with the bulk gap quantified by the Chern-Simons mass and conductivity mediated by the ballistic edge Cooper pair modes. At zero temperature, the transitions superinsulator $\leftrightarrow$ BM at g_1 and superconductor $\leftrightarrow$ BM at g_2 are BKT quantum phase transitions dual to each other so that $g_1 = 1/g_2$. At $\eta \to 1$ the two transitions merge into a self-dual quantum tricritical point at $(\eta = 1, g = 1)$ as shown in Fig. 3b. At $\eta < 1$ the direct SIT is a first order transition.

Equipped with these theory predictions, we turn to the analysis of the experimental data. Plotting $R_\square(B)$ for different temperatures above the saturation yields three near-crossing points at fields B_{SB}, B_{SI}, B_{IB} and corresponding resistances R_{SB}, R_{SI}, R_{IB}, see Fig. 4c. To verify our central prediction about the quantum phase transitions (QPT) we perform a scaling analysis. The scaling theory of a QPT involves a diverging spatial correlation length ξ_{QPT} and a correlation time τ, related via $\xi_{QPT} \propto \tau^z$ [37]. A quantum BKT transition implies $\xi_{QPT} \propto \exp(\text{const}/\sqrt{|g - g_c|})$, therefore one has to accordingly modify the standard finite size scaling formulae, noticing that now the substitution $\tau \to T_0/T$ yields the scaling variable $X = |g - g_c| \ln^2(T_0/T)$ replacing the standard one [37] $|g - g_c|/T^{1/z\nu}$, see SI for a detailed derivation. Here T_0 is a non-universal parameter determined by best fit. This BKT scaling can be viewed as a formal $\nu \to \infty$ limit of the original Fisher form, reflecting the fact that the BKT transition is an infinite-order transition. The BKT scaling is the exact opposite of the Griffith singularity scenario, in which $z \to \infty$, rather than ν. The Griffith scenario is associated with strong disorder. In our case, instead, the Harris criterion [43], implies that disorder is irrelevant for the SIT in the renormalization group sense. The role of disorder in the large-scale properties of the system is merely to tune the SIT and renormalize material parameters.

We plot $R_\square(B, T)$ as a function of X around B_{SB} and B_{IB}, identifying them as SC $\leftrightarrow$ BM and SI $\leftrightarrow$ BM transitions and treating T_0 as a fitting parameter optimizing the scaling curve. Figs. 4d,f demonstrate excellent scaling, spanning nearly two orders of magnitude of resistance at temperatures above 0.1 K, with the best fit achieved for $T_0 = 2$ K. In full concert with duality considerations, T_0 comes out the same for both transitions. Scaling survives also near B_{SI}, Fig. 4e due to the critical vicinity of the quantum tricritical point. The best scaling is achieved for $T_0 = 1$ K, again in accord with the theoretical expectation that for the tricritical point the parameter T_0 is expected to differ from those for SC $\leftrightarrow$ BM and SI $\leftrightarrow$ BM. We stress here that the criticality around B_{SI} is the criticality related to the tricritical point, since for $\eta < 1$ the

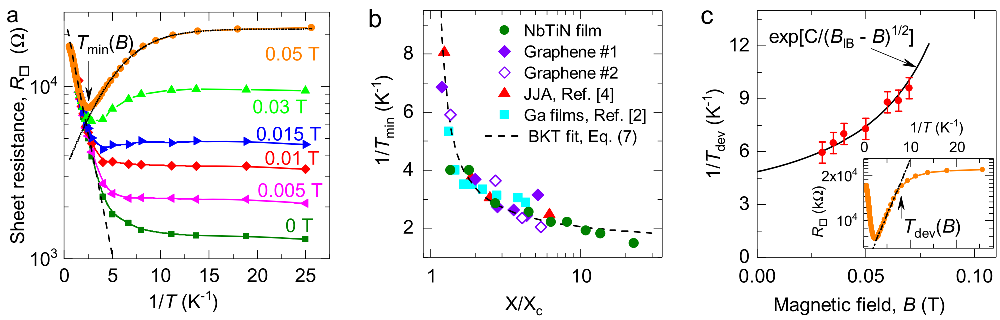

Fig. 5. Sheet resistance vs $1/T$ plots and the BKT scaling for correlation lengths. a: Representative $\log R_\square$ vs. $1/T$ plots. The dashed black line depicts $R \propto \exp(-T^*/T)$ dependence. The dotted line describes $R_\square(1/T)$ behavior for two parallel resistors comprising $R_b \propto \exp(T^{**}/T)$ (bulk modes) insulating dependence and constant (edge ballistic modes) behavior, see text. **b:** The BKT scaling of $1/T_{min} \sim \xi_{corr} \sim \exp[\text{const}/(X/X_c - 1)^{1/2}]$ of the BKT correlation length near the superconductor-BM quantum BKT transition in different materials driven by either magnetic field, disorder, or gate voltage, demonstrating the universality of the BKT superconductor-BM transition. The circles stand for $T_{min}(B)$ in NbTiN films, $X/X_c = B/B_{SB}$; the diamonds mark data for Van der Waals heterostructures of twisted double bilayer graphene (TDBG) where the SIT is tuned by the in-plane magnetic field, $X/X_c = B_{||}/B_c$, $B_c = 2.5$ T is an adjustment parameter and T_{min} is divided by 35; the triangles mark data for the SIT driven by the frustration factor $f = \Phi/\Phi_0$, with Φ being the magnetic flux per plaquette in JJA, $f_c = 0.1$ [4], and squares mark the film thickness driven SIT in granular films [2], for which $X/X_c = R_N/R_{Nc}$, $R_{Nc} = 32$ kΩ, T_{min} is divided by 16. **c:** The BKT scaling of the correlation length $\sim 1/T_{dev}$ near the insulator-Bose metal transition, detected by deviation of the resistance from the exponential insulating $\exp(T^{**}/T)$ behavior (the dashed line in the inset).

transition is of first-order and for $\eta > 1$ there is an intermediate BM phase. The scaling at this unique SIT point exhibits the BKT criticality, contrasting the ordinarily employed power-law scaling. This follows from the fact that, since in the critical vicinity of the tricritical point ($g = 1, \eta = 1$) two out of three merging phase transitions are of the BKT nature, the SIT tricritical point should also exhibit the BKT criticality [44]. This calls for revisiting all the rich lore of the experimental SIT and for careful re-inspection of its scaling behaviour. One immediately observes that the expected duality relations $B_{SB}/B_{SI} = B_{SI}/B_{IB}$ and $R_{SB}/R_{SI} = R_{SI}/R_{IB}$, are satisfied with good accuracy. This accuracy is an additional indication of the topological nature of the anomalous metal appearing between the insulating and superconducting phases at the SIT.

Shown in Fig. 5a are the magnified $R_\square(T)$ dependencies which we re-plotted as functions of $1/T$ for the fields below 0.16 T. We present a few representative curves to avoid data crowding. At relatively high temperatures one sees the resistance rapidly dropping as function of $1/T$ due to thermally activated vortex motion, $R_\square(1/T) \propto \exp(-T^*/T)$, the exponential behavior is shown by dashed line. At fields, $B < B_{SB}$, the resistance $R_\square(T)$ saturates at low temperatures, indicating the crossover to a quantum vortex creep regime (see SI). Our findings are in accord with the recently reported dissipative state with non-zero resistance in two-dimensional 2H-$NbSe_2$ films [45]. It is worth noting that, as is now well established, 2D quantum vortex creep is characteristic of a Cooper pair condensate state and, thus, B_{SB} does indeed denote the transition to a superconducting state. Above $B_{SB} = 0.011$ T the $R_\square(1/T)$ dependencies develop minima, which become less pronounced above the B_{SI} field, where the insulating behavior becomes dominant. These emergent minima signal that the bulk spectrum of charge excitations acquires a gap, which prevents bulk electronic transport. Such minima are often viewed as the hallmark of topological insulators, see, for example, [46] and references therein. We now note that in the BM, i.e. topological insulator domain, $B_{SB} < B < B_{IB}$, one can neglect the contribution from moving vortices as it is seen from Fig. 5a. Then the sheet resistance of the BM results from the charge current contribution from two parallel channels, (i) the ballistic edge modes and (ii) the thermally activated bulk modes over the CS gap. Accordingly, below the minimum, $T < T_{min}$, the sheet resistance is indeed perfectly fitted by the two parallel resistors formula $R_\square(T, B) = R_{CS}(T)R_{bal}(B)/[R_{CS}(T) + R_{bal}(B)]$, where $R_{CS}(T) \propto \exp(T_{CS}/T)$ is the bulk thermally activated resistance corresponding to surmounting the insulating gap T_{CS}, while $R_{bal}(B)$ is the field dependent resistance mediated by the edge modes. A fit for the field 0.05 T is shown by the dashed line in Fig. 4a. Upon increasing the magnetic field above $B_{SI} = 0.039$ T (i.e. moving into the $g < 1$ region), $R_{bal}(B)$ increases and the edge states incrementally mix with the bulk modes. As a result, the minimum in $R_\square(T, B)$ becomes less pronounced and the film crosses over continuously to insulating behavior. Markedly, the $R(T)$ vs. $1/T$ dependence in the TDBG exhibits remarkable similarity to that in NbTiN, see SI. It might be objected that detecting a topological insulator state with a magnetic field is not appropriate since this breaks the protecting time reversal symmetry of the edge modes, thereby inducing an edge gap. However, the magnitude of this gap can be estimated by the cyclotron frequency of the applied field. For our extremely weak fields this gives a gap always smaller than 25 mK even at the highest applied field values, and even much smaller typically. Since the lowest measurements temperatures were around 40 mK, the edge modes can be still considered as gapless in our whole experimental range.

Near the quantum BKT superconductor-BM and superinsulator-BM transitions the fugacities associated with the Cooper pair and vortex Bose condensates generate new energy scales and the corresponding correlation lengths $\xi_{SB} \sim 1/T_{min}$ and $\xi_{IB} \sim 1/T_{dev}$, respectively which are expected to display the BKT criticality. These energies are identified as T_{min}, the position of the minimum in $R_\square$, heralding the emergence of the bulk CS insulating gap, and the temperature T_{dev}, at which $R_\square(T)$ in Fig. 5a deviates from the insulating exponential dependence $\exp(\text{const}/T)$ and marking the switching on of the edge modes and the start of shunting the insulating bulk by metallic edge channels. The latter can be viewed as quantum wires, hence their switching on can be described as a BKT quantum phase transition in analogy to the seminal work [47]. Scaling of $1/T_{min}$ as function of the dimensionless tuning parameter B/B_{SI} is presented in Fig. 5b by green solid circles. Accordingly, the positions of the minima of $R(T)$ of TDBG at different $B_{||}$ are shown by violet diamonds. Also displayed in Fig. 5b are similar dependencies for other materials, metallic granular films [2] and JJA [4]. The data comply perfectly with the BKT exponential scaling illustrating the universality of the transition into the BM in different systems. The scaling of $1/T_{dev}$ is shown in Fig. 5c, although there the window of the magnetic fields is less wide and the error-bar near $B = B_{IB}$ grows large.

The presented gauge theory of the Bose metal reveals that the long-debated SIT-intervening metallic phase is a bosonic topological insulator. Its metallic conductance is mediated by bosonic edge modes and the superconductor-topological insulator and topological insulator-superinsulator transitions are quantum BKT phase transitions. The BKT scaling at the transition points, together with the high-precision duality relations for the transition fields and the corresponding resistances, providing an unambiguous evidence for the bosonic topological insulator and the associated quantum BKT transitions, are reported for the first time. Our observation of a bosonic topological insulator in NbTiN and similar behavior in TDBG, stresses its universal character as a result of the Chern-Simons gap in the spectrum of relevant excitations. Note that the occurrence of bosonic topological insulator in the double belayered graphene is in a concert with the expectations of [22]. Interestingly, our previous findings of [41] support also the percolation network picture [48] of gapless bosonic channels near the BKT transition to TI. Finally, our results resolve the long-standing puzzle of the SIT, unraveling that the system follows an indirect transition scenario through the intervening metallic state in systems with strong quantum fluctuations, while films with suppressed quantum fluctuations (more disordered and/or with the higher carrier densities) exhibit the direct SIT.

Materials and methods

Free energy We start with the action describing the intertwined vortex-CP dynamics derived in [20]:

$$S=\int dtd^2x\left[i\frac{\bar q}{2\pi}a_\mu\epsilon_{\mu\alpha\nu}\partial_\alpha b_\nu+\frac{v_c}{2e_{\rm v}^2}f_0f_0+\frac{1}{2e_{\rm v}^2v_c}f_if_i\right.$$
$$\left.+\frac{v_c}{2e_{\rm q}^2}g_0g_0+\frac{1}{2e_{\rm q}^2v_c}g_ig_i+i\sqrt{\bar q}a_\mu Q_\mu+i\sqrt{\bar q}b_\mu M_\mu\right], \qquad (8)$$

where $v_{\rm c}=1/\sqrt{\mu\varepsilon}$ is the speed of light in the film material, expressed in terms of the magnetic permeability μ and the electric permittivity ε (we use natural units $c=1$, $\hbar=1$). This action (8) is a non-relativistic version of the topologically massive gauge theory [21] describing a $(2+1)$-dimensional vector particle with the CS mass, $m_{\rm CS}=\bar q e_{\rm q}e_{\rm v}/2\pi v_c$, arising without spontaneous symmetry. The emergent gauge fields a_μ and b_μ mediate the mutual statistics interactions between Cooper pairs, with word-lines Q_μ and charge $\bar q=2$ and vortices of flux $2\pi/\bar q$, with world-lines M_μ. When appropriately regularized on a lattice of spacing ℓ (see Supplementary Information), these world-lines can be viewed as “strings” of typical length $L=N\ell$, carrying electric and magnetic quantum numbers Q and M, respectively. To derive the free energy of the interacting Cooper pair-vortex system the gauge fields in the above quadratic action are integrated out via the standard Gaussian integration procedure, obtaining thus an effective action for the charge and vortex strings alone. As usual in statistical field theory this has the interpretation of an energy for the “string gas”, which is proportional to the string length. To obtain a free energy associated with the strings, one has to include the contribution from the positional string entropy, which is also proportional to its length, with the proportionality factor $\mu_{\rm e}=\ln(5)$ representing the 5 possible choices for string continuation at each lattice site. For the relevant case of Cooper pairs (i.e. $\bar q=2$), we find the free energy in the main text.

Effective action for the topological insulator To determine the nature of the Bose metal we find its electromagnetic response by coupling the charge current $(\bar q e)j_\mu$ to an external electromagentic potential A_μ and we compute its effective action by integrating out gauge fields a_μ and b_μ,

$$e^{-S_{\rm eff}(A_\mu)}=\frac{1}{Z}\int\mathcal{D}a_\mu\mathcal{D}b_\mu e^{-S(a_\mu,b_\mu)+i(\bar qe)j_\mu A_\mu},$$
$$Z=\int\mathcal{D}a_\mu\mathcal{D}b_\mu e^{-S(a_\mu,b_\mu)}. \qquad (9)$$

This gives

$$S_{\rm eff}\left(A_\mu\right)=\frac{g}{4}\left(\frac{\bar qe}{2\pi}\right)^2d\int d^3x\left(v_cF_0^2+\frac{1}{v_c}F_i^2\right), \qquad (10)$$

where $F_\mu=\epsilon_{\mu\alpha\nu}\partial_\alpha A_\nu$ is the dual field strength and we have identified the geometric lattice factor $4\mu_e\eta\ell$ with the relevant thickness parameter d of the film, so as to maintain self-duality (see main text). This is the action of a bulk insulator which becomes best evident in the relativistic case, $v_c=1$:

$$S_{\rm eff}\left(A_\mu\right)=\frac{g}{2}\left(\frac{\bar qe}{2\pi}\right)^2d\int d^3x\,A_\mu\left(-\delta_{\mu\nu}\nabla^2+\partial_\mu\partial_\nu\right)A_\nu. \qquad (11)$$

Varying this action with respect to the vector potential A_ν gives the main text formula for the electric current.

Conduction by edge modes The Chern-Simons effective action is not invariant under gauge transformations $a_i=\partial_i\lambda$ and $b_i=\partial_i\chi$ at the edges. Two chiral bosons [34] $\lambda=\xi+\eta$ and $\chi=\xi-\eta$ have to be introduced to restore the full gauge invariance, exactly as it is done in the quantum Hall effect framework [35] and for topological insulators [49]. The full gauge invariance is restored by adding the edge action

$$S_{\rm edge}=\frac{1}{\pi}\int d^2x\,(\partial_0\xi\partial_s\xi-\partial_0\eta\partial_s\eta)+\bar qe_{\rm eff}\int d^2x\,A_0\left(\frac{\sqrt{\bar q}}{2\pi}\partial_s\chi\right), \qquad (12)$$

including the electromagnetic coupling of the edge charge density $\rho=(\bar qe_{\rm eff})(\sqrt{\bar q}/2\pi)\partial_s\chi$ in the $A_s=0$ gauge, $\bar qe_{\rm eff}$ being the effective charge of the Cooper pairs in the Bose metal phase, $\bar qe_{\rm eff}=\bar qe\sqrt{g}$. As in the case of the quantum Hall effect, the non-universal dynamics of the edge modes is generated by boundary effects [35], which result in the Hamiltonian

$$H=\frac{1}{\pi}\int ds\left[-v_b\left(\partial_s\xi\right)^2-v_b\left(\partial_s\eta\right)^2\right], \qquad (13)$$

where v_b is the velocity of propagation of the edge modes along the boundary. Upon adding this term, the total edge action becomes

$$S_{\rm edge}=\frac{1}{\pi}\int d^2x\,\left[\left(\partial_0-v_b\partial_s\right)\xi\partial_s\xi-\left(\partial_0+v_b\partial_s\right)\eta\partial_s\eta\right]$$
$$+\bar qe_{\rm eff}\int d^2x\,A_0\left(\frac{\sqrt{\bar q}}{2\pi}\partial_s\chi\right). \qquad (14)$$

The equation of motion generated by this action is

$$v_b\partial_s\rho=\frac{\bar qe_{\rm eff}}{2\pi}E=\frac{\bar qe_{\rm eff}}{2\pi}\partial_sA_0. \qquad (15)$$

Integrating this equation gives eq. (5) in the main text, which represent ballistic charge conduction with the resistance $R=R_{\rm Q}/g$.

Bose metal stability To analyze an intervening phase harboring dilute topological excitations in the Hamiltonian formalism, we set $Q_\mu=M_\mu=0$ and decompose the original gauge fields in Eq. (8) as $a^i=\partial_i\xi+\epsilon^{ij}\partial_j\phi$, $b^i=\partial_i\lambda+\epsilon^{ij}\partial_j\psi$. Quantizing the action in (8) we arrive at the ground state wave functional

$$\Psi[a^i,b^i]=\exp\left[i(\bar q/4\pi)\int d^2\mathbf{x}\,(\psi\Delta\xi+\phi\Delta\lambda)\right.$$
$$\left.-(\bar q/4\pi)\int d^2\mathbf{x}\left(g(\partial_i\phi)^2+\frac{1}{g}(\partial_i\psi)^2\right)\right],$$

generalizing the Schrödinger wave function to a system with an infinite number of degrees of freedom. The fields ϕ and ψ represent vortex- and CP charge-density waves, which are gapped due to the mutual statistics interactions. When the two symmetries are compact, however, the fields ξ and λ are angles and we have to take into account also the corresponding topological excitations, vortices and point charges. These can be in highly entangled mixed states or in their pure free state. Quantum operator expectation values in the entangled mixed state in which vortices are the non-observed environment, are given by $\langle\mathcal{O}\rangle \propto \int \mathcal{D}\psi\mathcal{D}\lambda\,\mathcal{O}(\psi,\lambda)\;\exp\big(-\int d^2\mathbf{x}\;\frac{\bar{q}}{2\pi g}(\partial_i\psi)^2 + \frac{\bar{q}}{2\pi g}(\partial_i\lambda)^2 - 2z\cos\lambda\big)$, see SI. The quantum fugacity z governs the degree of entanglement. This is the classical partition function of the sine-Gordon model undergoing the BKT transition [32,33]. In a quantum case, it is a quantum BKT transition at the "effective temperature" for vortex liberation set by the quantum conductance parameter g. Correspondingly, charge liberation from the dual entangled state is set by $1/g$. The highly entangled states correspond to superconductor and superinsulator at high and low values of g, respectively, where vortices and charges have algebraic correlation functions. The Bose topological insulator is the intervening state at $g \simeq 1$, where both charges and vortices are screened by strong quantum fluctuations, leading to correlation functions (7).

Samples and measurements To grow NbTiN films, we employed the atomic layer deposition (ALD) technique based on sequential surface reaction step-by-step film growth. The fabrication technique is described in detail in the Supplemental Material. This highly controllable process provides superior thickness and stoichiometric uniformity and an atomically smooth surface [50] as compared to chemical vapor deposition, the standard technique used to grow NbTiN films. We used $NbCl_5$, $TiCl_4$, and NH_3 as gaseous reactants; the stoichiometry was tuned by varying the ratio of $TiCl_4/NbCl_5$ cycles during growth [51]. The superconducting properties of these ultrathin NbTiN films were optimized by utilizing AlN buffer layers grown on top of the Si substrate [52]. $Nb_{1-x}Ti_xN$ films of thicknesses $d = 10$ were grown. Films have a fine-dispersed polycrystalline structure [41]. The average crystallite size is ≈ 5 nm. Deposition temperature is 350^0C. Ti fraction x is 0.3.

The films were lithographically patterned into bridges 50 μm wide, the distance between current-contacts was 2500 μm and distance between voltage-contacts was 450 μm. Most resistive transport measurements are carried out using low-frequency ac techniques in a two-terminal configuration with $V \approx 100$ μV, $f \approx 1$ Hz. Additionally we measured temperature dependence of resistance at zero magnetic field. Additionally we measured temperature dependence of resistance at zero magnetic field using both, two- and four-terminal, configurations. From comparison the obtained data we determined the number of squares in a two-terminal configuration for determining the resistance per square and the contact resistance. For ac measurements we use SR830 Lock-ins and current preamplifiers SR570. All the resistance measurement are carried out in linear regime with using adequately system of filtration. Resistivity measurements at sub-Kelvin temperatures were performed in dilution refrigerators ^{3}He/^{4}He with superconducting magnet.

Data availability

The original experimental data of this article are available upon request.

Declaration of competing interest

The authors declare that they have no known competing financial interests or personal relationships that could have appeared to influence the work reported in this paper.

Acknowledgements

We are delighted to thank Thomas Proslier for preparing NbTiN samples used in the experiments and Tom Rosenbaum for valuable discussions. M.C.D. thanks CERN, where she completed this work, for kind hospitality. S.V.P. is grateful to Tatyana Baturina for valuable contribution at the initial stage of work on NbTiN films. The work at Argonne (V.M.V.) was supported by the U.S. Department of Energy, Office of Science, Basic Energy Sciences, Materials Sciences and Engineering Division, the work at UOC (partially V.M.V) was supported by the NSF grant DMR-1809188. The work on transport measurements at Novosibirsk (A.Yu.M. and S.V.P.) was supported by Russian Science Foundation project No. 18-72-10056. The work of S.V.P. on the analysis of experimental data was supported by RFBR project No. 18-32-00718 mol-a. The work by Y.K. was supported by FAPESP, CNPq and AFOSR Grant FA9550-17-1-0132. The work at Caltech (D.S.) was supported by National Science Foundation Grant No. DMR-1606858.

Appendix A. Supplementary material

Supplementary material related to this article can be found online at https://doi.org/10.1016/j.physleta.2020.126570.

References

[1] D. Haviland, Y. Liu, A. Goldman, Onset of superconductivity in the two-dimensional limit, Phys. Rev. Lett. 62 (1989) 2180–2183.
[2] H.M. Jaeger, D.B. Haviland, B.G. Orr, A.M. Goldman, Onset of superconductivity in ultrathin granular metal films, Phys. Rev. B 40 (1989) 183–196.
[3] A. Hebard, M.A. Paalanen, Magnetic-field-tuned superconductor-insulator transition in two-dimensional films, Phys. Rev. Lett. 65 (1990) 927–930.
[4] H.S.J. van der Zant, F.C. Fritschy, W.J. Elion, L.J. Geerligs, J.E. Mooij, Field-induced superconductor-to-insulator transitions in Josephson-junction arrays, Phys. Rev. Lett. 69 (1992) 2971.
[5] N. Mason, A. Kapitulnik, Dissipation effects on the superconductor– insulator transition in 2D superconductors, Phys. Rev. Lett. 82 (1999) 5341–5344.
[6] N. Marković, C. Christiansen, A.M. Mack, W.H. Huber, A.M. Goldman, Superconductor–insulator transition in two dimensions, Phys. Rev. B 60 (1999) 4320–4328.
[7] M.A. Steiner, N.P. Breznay, A. Kapitulnik, Approach to a superconductor-to-Bose-insulator transition in disordered films, Phys. Rev. B 77 (2008) 212501.
[8] A.T. Bollinger, et al., Superconductor-insulator transition in $La_{2-x}Sr_xCuO_4$ at the pair quantum resistance, Nature 472 (2011) 458–460.
[9] S. Eley, S. Gopalakrishnan, P.M. Goldbart, N. Mason, Approaching zero-temperature metallic states in mesoscopic superconductor–normal–superconductor arrays, Nat. Phys. 8 (2012) 59–62.
[10] A. Allain, Z. Haz, V. Bouchiat, Electrical control of the superconductingto-insulating transition in graphene-metal hybrids, Nat. Mater. 11 (2012) 590–594.
[11] Z. Haz, et al., Collapse of superconductivity in a hybrid tin-graphene Josephson junction array, Nat. Phys. 10 (2014) 380–386.
[12] F. Couëdo, et al., Dissipative phases across the superconductor-to-insulator transition, Sci. Rep. 6 (2016) 35834.
[13] S. Park, J. Shin, E. Kim, Scaling analysis of field-tuned superconductor–insulator transition in two-dimensional tantalum thin films, Sci. Rep. 7 (2017) 42969.
[14] N.P. Breznay, A. Kapitulnik, Particle-hole symmetry reveals failed superconductivity in the metallic phase of two-dimensional superconducting films, Sci. Adv. 3 (2017) e1700612.
[15] C.G.L. Bottcher, et al., Superconducting, insulating and anomalous metallic regimes in a gated two-dimensional semiconductor-superconductor array, Nat. Phys. 14 (2018) 1138–1144.
[16] D. Das, S. Doniach, Existence of a Bose metal at $T = 0$, Phys. Rev. B 60 (1999) 1261–1275.
[17] A.M. Goldman, Superconductor-insulator transitions, Int. J. Mod. Phys. B 24 (2010) 4081–4101.
[18] A. Kapitulnik, S.A. Kivelson, B. Spivak, Anomalous metals – failed superconductors, Rev. Mod. Phys. 91 (2019) 011002.
[19] M.C. Diamantini, P. Sodano, C.A. Trugenberger, Gauge theories of Josephson junction arrays, Nucl. Phys. B 474 (1996) 641–677.
[20] M.C. Diamantini, C.A. Trugenberger, V.M. Vinokur, Confinement and asymptotic freedom with Cooper pairs, Commun. Phys. 1 (2018) 77.
[21] S. Deser, R. Jackiw, S. Templeton, Three-dimensional massive gauge theories, Phys. Rev. Lett. 48 (1982) 975.
[22] Z. Bi, et al., Bilayer graphene as a platform for bosonic symmetry-protected topological states, Phys. Rev. Lett. 118 (2017) 126801.

[23] T.I. Baturina, et al., Localized superconductivity in the quantum-critical region of the disorder-driven superconductor-insulator transition in TiN thin films, Phys. Rev. Lett. 99 (2007) 257003.
[24] V.M. Vinokur, et al., Superinsulator and quantum synchronization, Nature 452 (2008) 613–615.
[25] R. Ganguli, et al., Magnetic field induced emergent inhomogeneity in a superconducting film with weak and homogeneous disorder, Phys. Rev. B 96 (2017) 054509.
[26] M.C. Diamantini, C.A. Trugenberger, V.M. Vinokur, Topological gauge theory of the superconductor-insulator transition, in: Topological Phase Transitions and New Developments, World Scientific, 2019, p. 197.
[27] M.P.A. Fisher, G. Grinstein, Quantum critical phenomena in charged superconductors, Phys. Rev. Lett. 60 (1998) 208–211.
[28] M.-C. Cha, M.P.A. Fisher, S.M. Girvin, M. Vallin, A.P. Young, Phys. Rev. B 44 (1991) 6883–6902.
[29] P. Phillips, D. Davidovich, The elusive Bose metal, Science 302 (2003) 243–247.
[30] F. Wilczek, Disassembling anyons, Phys. Rev. Lett. 69 (1992) 132–135.
[31] R. Fazio, G. Schön, Charge and vortex dynamics in arrays of tunnel junctions, Phys. Rev. B 43 (1991) 5307–5320.
[32] V.L. Berezinskii, Destruction of long-range order in one-dimensional and two-dimensional systems having a continuous symmetry group. I. Classical systems, Sov. Phys. JETP 32 (1970) 493–500.
[33] J.M. Kosterlitz, D.J. Thouless, Long range order and metastability in two dimensional solids and superfluids. Application of dislocation theory, J. Phys. C, Solid State Phys. 5 (1972) L124.
[34] R. Floreanini, R. Jackiw, Self-dual fields as charge-density solitons, Phys. Rev. Lett. 59 (1987) 1873–1876.
[35] X-G. Wen, Theory of the edge states in fractional quantum hall effects, Int. J. Mod. Phys. B 6 (1992) 1711–1762.
[36] M.P.A. Fisher, G. Grinstein, S.M. Girvin, Presence of quantum diffusion in two dimensions: universal resistance at the superconductor-insulator transition, Phys. Rev. Lett. 64 (1990) 587–590.
[37] M.P.A. Fisher, Quantum phase transitions in disordered two-dimensional superconductors, Phys. Rev. Lett. 65 (1990) 923–926.
[38] Y-M. Lu, A. Vishwanath, Theory and classification of interacting integer topological phases in two dimensions: a Chern-Simons approach, Phys. Rev. B 86 (2012) 125119.
[39] C. Wang, T. Senthil, Boson topological insulators: a window into highly entangled quantum phases, Phys. Rev. B 87 (2013) 235122.
[40] T.I. Baturina, V.M. Vinokur, Superinsulator-superconductor duality in two dimensions, Ann. Phys. 331 (2013) 236–257.
[41] A.Y. Mironov, et al., Charge Berezinskii-Kosterlitz-Thouless transition in superconducting NbTiN films, Sci. Rep. 8 (2018) 4082.
[42] X. Liu, et al., Spin-polarized correlated insulator and superconductor in twisted double bilayer graphene, arXiv:1903.08130v2, 2019.
[43] A.B. Harris, Upper bounds for the transition temperatures of generalized Ising models, J. Phys. C 7 (1974) 1671.
[44] J. Zinn-Justin, Quantum Field Theory and Critical Phenomena, Clarendon Press, Oxford, 1989.
[45] A. Benyamini, et al., Fragility of the dissipationless state in clean two-dimensional superconductors, Nat. Phys. 15 (2019) 947–953.
[46] K. Wang, D. Graf, L. Li, L. Wang, C. Petrovic, Anisotropic giant magnetoresistance in $NbSb_2$, Sci. Rep. 4 (2015) 7328.
[47] P. Bobbert, R. Fazio, G. Schon, A.D. Zaikin, Phase transitions in dissipative Josephson chains: Monte Carlo results and response functions, Phys. Rev. B 45 (1992) 2294–2304.
[48] J.T. Chalker, P.D. Coddington, Percolation, quantum tunnelling and the integer Hall effect, J. Phys. C 21 (1988) 2665–2679.
[49] G.Y. Cho, J.E. Moore, Topological BF field theory description of topological insulators, Ann. Phys. 326 (2011) 1515–1535.
[50] B.S. Lim, A. Rahtu, R.G. Gordon, Atomic layer deposition of transition metals, Nat. Mater. 2 (2003) 749–754.
[51] T. Proslier, J.A. Klug, N.C. Becker, J.W. Elam, M.J. Pellin, Atomic layer deposition of superconductors, ECS Trans. 41 (2011) 237.
[52] T. Shiino, et al., Improvement of the critical temperature of superconducting NbTiN and NbN thin films using the AlN buffer layer, Supercond. Sci. Technol. 23 (2010) 045004.